




# $H_0$ Reconstruction with Type Ia Supernovae, Baryon Acoustic Oscillation and Gravitational Lensing Time Delay

Meng-Zhen Lyu<sup>1</sup> , Balakrishna S. Haridasu<sup>2,3</sup>, Matteo Viel<sup>4,5,6,7</sup>, and Jun-Qing Xia<sup>1</sup><sup>1</sup> Department of Astronomy, Beijing Normal University, Beijing 100875, People's Republic of China; [lvmz@mail.bnu.edu.cn](mailto:lvmz@mail.bnu.edu.cn), [xiajq@bnu.edu.cn](mailto:xiajq@bnu.edu.cn)<sup>2</sup> Dipartimento di Fisica, Università di Roma "Tor Vergata", Via della Ricerca Scientifica 1, I-00133, Roma, Italy; [haridasu@roma2.infn.it](mailto:haridasu@roma2.infn.it)<sup>3</sup> Sezione INFN, Università di Roma "Tor Vergata", Via della Ricerca Scientifica 1, I-00133, Roma, Italy<sup>4</sup> SISSA-International School for Advanced Studies, Via Bonomea 265, 34136 Trieste, Italy; [viel@sisssa.it](mailto:viel@sisssa.it)<sup>5</sup> INFN, Sezione di Trieste, Via Valerio 2, I-34127 Trieste, Italy<sup>6</sup> INAF—Osservatorio Astronomico di Trieste, Via G.B. Tiepolo 11, I-34143 Trieste, Italy<sup>7</sup> IFPU, Institute for Fundamental Physics of the Universe, via Beirut 2, 34151 Trieste, Italy

Received 2020 January 30; revised 2020 June 30; accepted 2020 July 16; published 2020 September 11

## Abstract

There is a persistent  $H_0$ -tension, now at more than  $\gtrsim 4\sigma$  level, between the local distance ladder value and the Planck cosmic microwave background measurement, in the context of flat Lambda-cold-dark-matter ( $\Lambda$ CDM) model. We reconstruct  $H(z)$  in a cosmological-model-independent way using three low-redshift distance probes including the latest data from baryon acoustic oscillation, supernova Ia (SN Ia) and gravitational lensing time-delay (GLTD) observations. We adopt general parametric models of  $H(z)$  and assume a Gaussian sound horizon at drag epoch,  $r_s$ , from Planck measurement. The reconstructed Hubble constant  $H_{0,\text{rec}}$  using Pantheon SN Ia and Baryon Acoustic Oscillations (BAO) data are consistent with the Planck flat  $\Lambda$ CDM value. When including the GLTD data,  $H_{0,\text{rec}}$  increases mildly, yet remains discrepant with the local measurement at  $\sim 2.2\sigma$  level. With our reconstructions being blind to the dark sectors at low redshift, we reaffirm the earlier claims that the Hubble tension is not likely to be solved by modifying the energy budget of the low-redshift universe. We further forecast the constraining ability of future realistic mock BAO data from Dark Energy Spectroscopic Instrument and GLTD data from Large Synoptic Survey Telescope, combining which, we anticipate that the uncertainty of  $H_{0,\text{rec}}$  would be improved by  $\sim 27\%$ , reaching  $\sigma_{H_{0,\text{rec}}} \approx 0.67$  uncertainty level.

*Unified Astronomy Thesaurus concepts:* [Observational cosmology \(1146\)](#); [Distance indicators \(394\)](#); [Strong gravitational lensing \(1643\)](#); [Type Ia supernovae \(1728\)](#)

## 1. Introduction

The flat Lambda-cold-dark-matter ( $\Lambda$ CDM) model is a remarkably successful cosmological model. It describes many observational results well, especially at large scales, including the cosmic microwave background (CMB) radiation, light element abundance as the relic of big bang nucleosynthesis, galaxy clustering, Ly $\alpha$  forest observations and also distance from low-redshift probes. However, there exists a strong tension for the present Hubble expansion rate ( $H_0$ ), between the direct measurement using distance ladder of local universe (Riess et al. 2016, 2019; Yuan et al. 2019), and the Planck estimate (Ade et al. 2016; Aghanim et al. 2018) from CMB within the context of  $\Lambda$ CDM (Bernal et al. 2016; Raveri & Hu 2019; Verde et al. 2019). One important aspect is that the discordance, since the first release of Planck data (Ade et al. 2014), has become even more prominent due to the improved precision of both measurements, which are at  $\sim 9\%$  difference, now reaching a significance of  $\gtrsim 4\sigma$  (Riess et al. 2019). More recent low-redshift GLTD measurements, independent of the local distance ladder, also shows a tension at high significance (Wong et al. 2020). The  $H_0$  tension, persisting and severely increasing, indicates that it should not merely be regarded as a statistical fluctuation, and is more likely to point to a failure of the standard  $\Lambda$ CDM model, as also noted in Verde et al. (2019), or due to unknown systematics in the data.

CMB provides a stringent constraint on  $H_0$  by combining the measurements of angular location and relative height of the acoustic oscillation of the baryon-photon fluid frozen at last scattering surface at  $z \approx 1100$ . However, the measurement is

model-dependent and influenced by possible extensions to the  $\Lambda$ CDM model, such as the dark energy equation of state parameter  $w$ <sup>8</sup> or the curvature  $\Omega_k$ , which as is well-known further aggravates the tension. Thus, modifying either the early or the local universe physics can, in principle, alter the  $H_0$  constraints from CMB measurements.

Modification to the  $\Lambda$ CDM model often involves ingredients beyond the standard physics, although the existence of dark matter and dark energy within the  $\Lambda$ CDM framework has already established the necessity for “new” physics. Preferable approaches can be to the modified dark energy model and different gravitational field behavior (Umiltà et al. 2015; Ballardini et al. 2016; Huang & Wang 2016; di Valentino et al. 2017a, 2018b; Zhao et al. 2017; Poulin et al. 2018; Banihashemi et al. 2019; Choi et al. 2019; Khosravi et al. 2019; Rossi et al. 2019), such as an early dark energy (Xia & Viel 2009; Karwal & Kamionkowski 2016; Mortsell & Dhawan 2018; Poulin et al. 2019; Ye & Piao 2020), interaction between dark sectors (Ko & Tang 2016; Raveri et al. 2017; di Valentino et al. 2018a; Archidiacono et al. 2019), interacting dark energy model (Xia et al. 2013; Kumar & Nunes 2016; di Valentino et al. 2017b; Yang et al. 2018; Pan et al. 2019), and a family of unified dark matter models (e.g., Camera et al. 2019 and references therein). Apart from the cosmological models,

<sup>8</sup> One possible way to relieve the Hubble tension is allowing phantom dark energy (di Valentino et al. 2017a; Vagnozzi 2020). This might, however, have a discrepancy with the low-redshift BAO measurements, which constrains better the  $w \lesssim -1$  range, see, e.g., Bernal et al. (2016), Aubourg et al. (2015), Haridasu et al. (2018b), and Park & Ratra (2019).

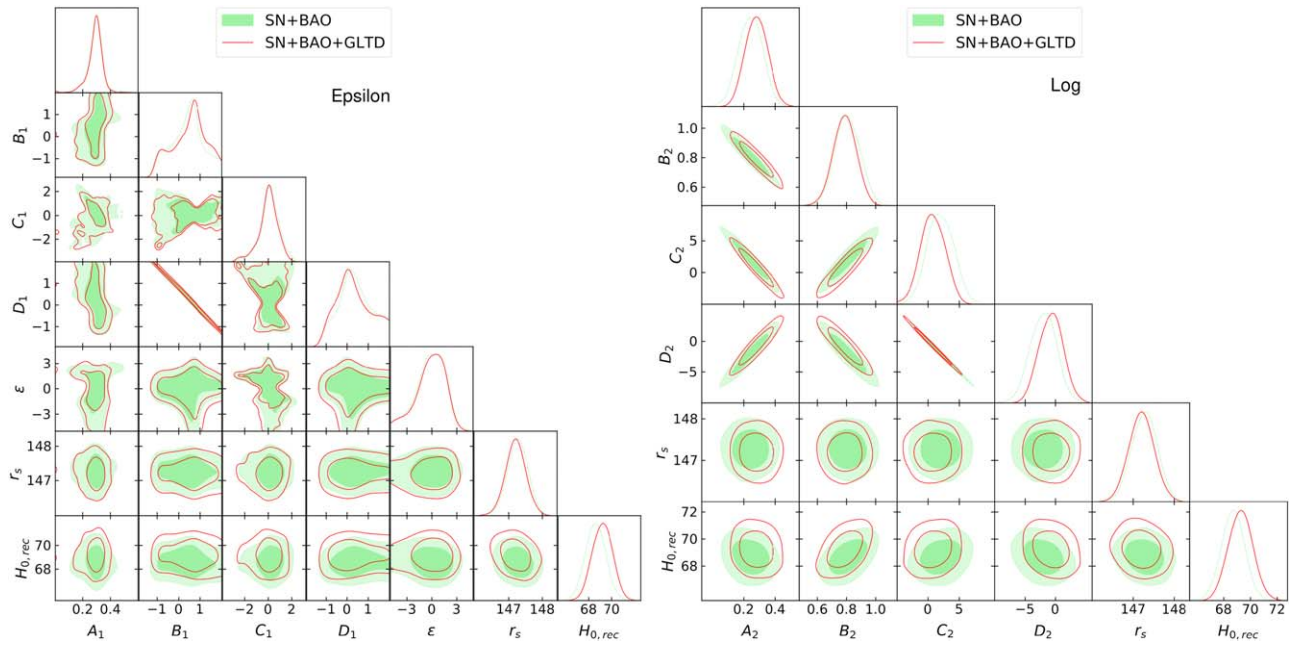


**Figure 1.** Left panel: parameter constraints for the the Epsilon model at the 68% and 95% confidence levels (CLs). Right panel: same as left, but for the Log model. In both the panels we also show  $H_{0,rec}$ , which is a derived quantity.

local gravitational potential (Marra et al. 2013), specifically a local void (Keenan et al. 2013; Whitbourn & Shanks 2014) can also partially relieve  $H_0$  tension (Hoscheit & Barger 2017; Shanks et al. 2019), yet there are studies utilizing supernova (SN) data sets (Kenworthy et al. 2019; Luković et al. 2020), which show that the local structure does not significantly impact the measurement of  $H_0$ .

Before we turn to revamp the standard  $\Lambda$ CDM model, it is necessary to get some insight from low-redshift cosmological probes, whose variability and observational accuracy can provide us an integrated and precise understanding of the late universe. In this work, we perform a cosmological-model-independent reconstruction of  $H(z)$ , an inverse distance ladder analysis using the SNe Ia, Baryon Acoustic Oscillations (BAO), and GLTD data, which are able to impose a strong constraint on the shape of  $H(z)$ . We include the GLTD data as it is independent of BAO and SN Ia. Although its current uncertainties are not comparable to the latter, it has the advantage of measuring the absolute distances, unlike the SN Ia, which needs marginalization of the nuisance parameter, i.e., standardized absolute luminosity.

Our analyses are closely related to the recent work by (Lemos et al. 2019; hereafter L18) while we update the BAO data and include the GLTD data into analyses. We found no evidence of non-zero curvature and deviation from the  $\Lambda$ CDM model in terms of the reconstructed  $H(z)$  while in fact the  $\Lambda$ CDM model performs better according to the Deviance Information Criterion (DIC). Our inferred  $H_0$  when combining all three probes is slightly higher than the primary results of L18, which is mostly due to the inclusion of GLTD data whose estimate of  $H_0$  is higher than the one from the Planck  $\Lambda$ CDM. As a more important extension, we forecast the performance of future BAO data from the Dark Energy Spectroscopic Instrument (DESI; Levi et al. 2013) and GLTD data from the Large Synoptic Survey Telescope (LSST; Ivezić et al. 2019). We conservatively expect the constraint on  $H_{0,rec}$

can reach up to  $\approx 0.67$  uncertainty level when combining the forthcoming data from these two surveys.

The paper is organized as follows: in Section 2 we introduce the parametric form of  $H(z)$ . In Section 3, we present the data used for reconstruction as well as the inference method. We show the final results using the current and future data in Section 4 and then follow the discussion and summary in Section 5.

## 2. Model and Equations

First, we parameterize  $H(z)$  in the following two ways:

$$\left(\frac{H(z)}{H_{0,fid}}\right)^2 = A_1(1+z)^3 + B_1 + C_1z + D_1(1+z)^\epsilon, \quad (1)$$

$$\left(\frac{H(z)}{H_{0,fid}}\right)^2 = A_2(1+z)^3 + B_2 + C_2z + D_2 \ln(1+z), \quad (2)$$

which are the same as in L18, and denote them as Epsilon model and Log model, respectively. While these models serve the purpose of being blind to the dark energy equation of state, they are clearly inadequate to account for the curvature freedom. Moreover, ignoring the curvature would induce error that grows rapidly with redshift in reconstructing the dark energy equation of state (Clarkson et al. 2007). To accommodate for this we also implement two additional models:

$$\left(\frac{H(z)}{H_{0,fid}}\right)^2 = A_3(1+z)^3 + B_3(1+z)^2 + C_3 + D_3 \ln(1+z), \quad (3)$$

$$\left(\frac{H(z)}{H_0}\right)^2 = A_4(1+z)^3 + B_4(1+z)^2 + D_4. \quad (4)$$

They are denoted as the Log2 model and  $\Omega_k\Lambda$ CDM model, respectively. We substitute the term  $\propto z$  with a  $\propto(1+z)^2$  term

for theoretical and practical reasons: (i) the latter has cosmological implication for the curvature of the universe, (ii) as shown in the right panel of Figure 1, the parameters  $C_2$  and  $D_2$  are strongly correlated, which is primarily due to  $\ln(1+z) \approx z$  at small redshifts. We also implement the  $\Omega_k \Lambda$ CDM model, which we write in a similar parametric form while putting two restrictions on its parameters: (i)  $H_0$  is a free parameter, which is a different implementation from other models where  $H_{0,\text{rec}}$  is a derived quantity, (ii)  $A_4 + B_4 + D_4 = 1$ , which is in fact the consistency relation when rewritten in terms of standard density parameters ( $\Omega_m + \Omega_k + \Omega_\Lambda = 1$ ). We adopt a fiducial Hubble constant value of  $H_{0,\text{fid}} = 67.0$ ,  $\text{km s}^{-1} \text{Mpc}^{-1}$ . The reconstructed  $H_0$ , denoted as  $H_{0,\text{rec}}$ , for each model is deduced at  $z=0$  after extrapolation. The choice of  $H_{0,\text{fid}}$  does not alter  $H_{0,\text{rec}}$ .<sup>9</sup>

In both Log2 and  $\Omega_k \Lambda$ CDM model, having the explicit  $(1+z)^2$  term, which has the interpretation of cosmic curvature, the transverse comoving distance  $D_M$  becomes

$$D_M(z) = \begin{cases} \frac{D_H}{\sqrt{\Omega_k}} \sinh\left(\frac{\sqrt{\Omega_k} D_C(z)}{D_H}\right), & \Omega_k > 0 \\ D_C(z), & \Omega_k = 0, \\ \frac{D_H}{\sqrt{-\Omega_k}} \sin\left(\frac{\sqrt{-\Omega_k} D_C(z)}{D_H}\right), & \Omega_k < 0 \end{cases} \quad (5)$$

where the comoving distance  $D_C = c \int_0^z \frac{dz'}{H(z')}$  and  $D_H = c/H_{0,\text{rec}}$ ,  $c$  is the speed of light. For the Log2 model,  $\Omega_k$  is equivalent to  $B_3 H_{\text{fid}}^2 / H_{0,\text{rec}}^2$  and for  $\Omega_k \Lambda$ CDM it is  $B_4$ . Thus, the luminosity distance  $D_d$  and angular diameter distance  $D_A$  are

$$D_L(z) = D_M(z)(1+z), \quad D_A(z) = D_M(z)/(1+z), \quad (6)$$

and the effective volume averaged distance, denoted as  $D_V$ , which often appears in BAO measurements, is defined as:

$$D_V(z) = \left[ D_M^2(z) \frac{cz}{H(z)} \right]. \quad (7)$$

The comoving sound horizon at drag epoch,  $z_s$ , is defined as

$$r_s(z_s) = c_s \int_{z_s}^{\infty} \frac{dz'}{H(z')}. \quad (8)$$

The sound velocity  $c_s$  is a function of the ratio of baryon to photon energy density ( $\rho_b/\rho_\gamma$ ). Our purpose here is to reconstruct  $H(z)$  in a model-independent way, having minimum involvement with the physics of the early universe. Therefore, we use the measurement of  $r_s$  from the Planck (Ade et al. 2016), which implies we assume the universe before  $z_s$  is the same as depicted by the  $\Lambda$ CDM model. Also, it has been shown that the dark energy and curvature degree of freedom do not modify the expectation of  $r_s(z_s)$  (Verde et al. 2017a, 2017b). The  $H(z)$  parameterizations in Equations (1)–(3) are valid only in the late universe.

In a strong lens system, light from a background object is bent by an intervening mass (lens), and multiple images are generated. Usually, these light rays go through different optical

paths when passing the gravitational potential of the lens due to complicate morphologies of the system. If the source happens to have a variation in flux, then the difference in optical paths finally turn out to be the difference in the arrival time, i.e., the time delay, of the photon from the images to us. This time delay conveys a combination of distance information of the lens system, which is called as the time-delay distance and denoted as  $D_{\Delta t}$  (Narayan 1991; Treu & Marshall 2016), reads

$$D_{\Delta t} = (1+z_l) \frac{D_d D_s}{D_{ls}}, \quad (9)$$

where  $z_l$  is the redshift of the lens, and  $D_d$  and  $D_s$  are the angular diameter distance from us to the lens and source, respectively.  $D_{\Delta t}$  has the dimension of distance and consequently is inversely proportioned to  $H_0$ . Moreover, with a proper assumption of lens mass density profile, one can extract  $D_d$  by combining the lens stellar velocity dispersion measurements and time-delay measurements (Paraficz & Hjorth 2009; Jee et al. 2015).

### 3. Data Sets and Inference Method

Our work is based on the following three probes: SN Ia, BAO, and GLTD. In this section, we first summarize in detail the data used here and then we present the inference method for our reconstruction of  $H(z)$ .

#### 3.1. Data Sets

- SN Ia from the Pantheon sample (Scolnic et al. 2018) which contains a total of 1048 SN Ia spanning the redshift range from  $0.01 < z < 2.3$ . The Pantheon sample is a large combination of SN Ia from various surveys and has unique advantages in its large sample number and wide redshift range for studying the expansion history, and it has consistent constraints on physics of the late universe, such as the dark energy, with that from the joint light-curve analysis SN Ia (Betoule et al. 2014) and also the latest Dark Energy Survey Supernova Program SN Ia sample (Abbott et al. 2019).
- Table 1 summarizes the latest BAO measurements used in this paper. They are measurements from 6dF Galaxy Survey (6dFGS; Beutler et al. 2011), BOSS DR12 in three redshift bands (Alam et al. 2017) and three high-redshift BAO measurements from eBOSS DR14 quasar (Zarrouk et al. 2018), Ly $\alpha$  absorption in the quasar spectrum (Blomqvist et al. 2019), and Ly $\alpha$ -quasar cross-correlation (de Sainte Agathe et al. 2019). Measurements from eBOSS DR14 luminosity red galaxies at  $z_{\text{eff}} = 0.72$  (IcazaLizaola et al. 2020) are excluded for the relative low constraining power and small correlation of  $\sim 0.16$  (Bautista et al. 2018) with the last data point in BOSS DR12.
- The BOSS DR14 Ly $\alpha$  and QSO  $\times$  Ly $\alpha$  data has been included in the current version of CosmoMC package (later introduced in Section 3.2) where the likelihoods for BAO peak-position parameters  $\alpha_{\parallel}$  and  $\alpha_{\perp}$  are used. The  $H(z_{\text{eff}})$ s listed in Table 1 are used to plot Figure 3. However, for the eBOSS DR14 QSO, since its likelihoods is still unavailable, we keep in line with L18, i.e., assume its measurements of  $H(z_{\text{eff}})$  and  $D_M$  are Gaussian and independent.
- We use six GLTD distance measurements as summarized in Table 2. They are, respectively, the analytic fit of  $P(D_{\Delta t})$  (Suyu et al. 2010) and  $P(D_d)$  (Jee et al. 2019) of

<sup>9</sup> We verify that a different assumption of  $H_{0,\text{fid}}$  hardly varies the inferred  $H_{0,\text{rec}}$  if we replace  $H_{0,\text{fid}} = 67.0$ ,  $\text{km s}^{-1} \text{Mpc}^{-1}$  with a different value, such as  $H_{0,\text{fid}} = 73.0$ ,  $\text{km s}^{-1} \text{Mpc}^{-1}$ .

**Table 1**  
Summary of BAO Data

Data Set	$z_{\text{eff}}$	Measurements	Constraint	Unit	Reference
6dFGS	0.106	$r_s/D_V(z_{\text{eff}})$	$0.336 \pm 0.015$	...	Beutler et al. (2011)
BOSS DR12	0.38	$D_M(z_{\text{eff}})r_{s,\text{fid}}/r_s$	$1512 \pm 25$	Mpc	Alam et al. (2017)
		$H(z_{\text{eff}})r_s/r_{s,\text{fid}}$	$81.2 \pm 2.4$	$\text{km s}^{-1} \text{Mpc}^{-1}$	
	0.51	$D_M(z_{\text{eff}})r_s/r_{s,\text{fid}}$	$1975 \pm 30$	Mpc	
		$H(z_{\text{eff}})r_s/r_{s,\text{fid}}$	$90.9 \pm 2.3$	$\text{km s}^{-1} \text{Mpc}^{-1}$	
eBOSS DR14 QSO	0.61	$D_M(z_{\text{eff}})r_s/r_{s,\text{fid}}$	$2307 \pm 37$	Mpc	Zarrouk et al. (2018)
		$H(z_{\text{eff}})r_s/r_{s,\text{fid}}$	$99.0 \pm 2.5$	$\text{km s}^{-1} \text{Mpc}^{-1}$	
		$D_A(z_{\text{eff}})r_{s,\text{fid}}/r_s$	$1850^{+90}_{-115}$	Mpc	
BOSS DR14 Ly $\alpha$	2.34	$D_M(z_{\text{eff}})/r_s$	$37.41 \pm 1.86$	...	Blomqvist et al. (2019)
		$c/(H(z_{\text{eff}})r_s)$	$8.86 \pm 0.29$	...	
BOSS DR14 QSO $\times$ Ly $\alpha$	2.35	$D_M(z_{\text{eff}})/r_s$	$36.3 \pm 1.8$	...	de Sainte Agathe et al. (2019)
		$c/(H(z_{\text{eff}})r_s)$	$9.20 \pm 0.36$	...	

**Note.**  $z_{\text{eff}}$  is the effective redshift of the BAO measurement.  $r_{s,\text{fid}} = 147.78$  Mpc is the fiducial sound horizon. We use the BAO peak-position parameters  $\alpha_{\parallel}$  and  $\alpha_{\perp}$  of the BOSS DR14 Ly $\alpha$  and QSO  $\times$  Ly $\alpha$  data from CosmoMC while for eBOSS DR14 QSO, since its inaccessibility of likelihood, we use the measurements list here directly.

**Table 2**  
Summary of GLTD Data

Lens Name	$z_d$	$z_s$	$D_{\Delta r}$ (Mpc)	$D_d$ (Mpc)	Type of Data	Reference(s)
B1608 + 656	0.6304	1.394	$5156^{+296}_{-236}$	$1228^{+177}_{-151}$	analytic fit	Suyu et al. (2010), Jee et al. (2019)
RXJ1131-1231	0.295	0.654	$2096^{+98}_{-83}$	$804^{+141}_{-112}$	MCMC chains	Suyu et al. (2014), Chen et al. (2019)
SDSS 1206 + 4332	0.7545	1.789	$5769^{+589}_{-471}$	$1805^{+555}_{-398}$		Birrer et al. (2019)
HE 0435-1223	0.4546	1.693	$2707^{+183}_{-168}$	...		Wong et al. (2016), Chen et al. (2019)
WFI2033-4723	0.6575	1.662	$4784^{+399}_{-248}$	...		Rusu et al. (2020)
PG 1115 + 080	0.311	1.722	$1470^{+137}_{-127}$	$697^{+186}_{-144}$		Chen et al. (2019)

**Note.** Units of distances are all Mpc (Jee et al. 2019).

B1608 + 656, the MCMC (Monte Carlo Markov chains) chains of  $D_{\Delta r}$  (if available) and  $D_d$  for RXJ1131-1231 (Suyu et al. 2014; Chen et al. 2019), SDSS 1206 + 4332 (Birrer et al. 2019), HE 0435-1223 (Wong et al. 2016; Chen et al. 2019), WFI2033-4723 (Rusu et al. 2020) and PG 1115 + 080 (Chen et al. 2019). The GLTD data can be obtained from the H0LiCOW website.<sup>10</sup>

The analytic likelihood function of distance  $D$  ( $D_{\Delta r}$  or  $D_d$ ) can be approximated as skewed log-normal distribution. The general expression is:

$$P(D|\theta) \approx \frac{1}{\sqrt{2\pi}(x - \lambda_D)\sigma_D} \times \exp\left[-\frac{(\log(x - \lambda_D) - \nu_D)^2}{2\sigma_D^2}\right], \quad (10)$$

where  $\theta$  is the model parameter vector.  $x$  is the model prediction of  $D$  ( $1 \text{ Mpc}^{-1}$ ). For B1608 + 656,  $\lambda_D$ ,  $\nu_D$  and  $\sigma_D$  for  $D_{\Delta r}$  are 4000.0, 7.053 and 0.228 while for  $D_d$  they are 334.2, 6.79671 and 0.1836.  $P(D_{\Delta r}|\theta)$  and  $P(D_d|\theta)$  are uncorrelated and can be multiplied directly (Wong et al. 2020).

For the other five GLTD observations, we first want to get the posterior probability density function (PDF) at arbitrary distance(s). In Wong et al. (2020), it is implemented via the kernel density estimator (KDE) from MCMC chains directly while here, we need some detours: we divide distance(s) into small bins and calculate PDF at these divide-points using KDE, i.e., we actually transfer those MCMC chains into discrete PDF at those points, which allows us to obtain the PDF at any distance(s) via interpolation. For the bin width, we adopt a value slightly smaller than the bandwidth of KDE, which is enough to keep as much distance distribution information from MCMC chains as that when using KDE directly. Using this method, for a flat  $\Lambda$ CDM cosmology with uniform priors on  $H_0 \subset [0, 150]$  and  $\Omega_M \subset [0.05, 0.5]$ , we get a consistent constraint on the marginalized  $H_0$  ( $=73.22 \pm 1.72$ ,  $\text{km s}^{-1} \text{Mpc}^{-1}$ ) with the one shown in Wong et al. (2020), which further guarantees our method correctly extracts the original distance information.

4. We use the measurement of  $r_s$  from the Planck 2015 TT, TE,EE+lowP likelihood combinations (Ade et al. 2016),

$$r_s = 147.27 \pm 0.31 \text{ Mpc}(68\% \text{ C.L.}). \quad (11)$$

<sup>10</sup> H0LiCOW Data Products ([https://shsuyu.github.io/H0LiCOW/site/holicow\\_data.html](https://shsuyu.github.io/H0LiCOW/site/holicow_data.html)) and a snapshot (<https://github.com/yooahin/HZ-reconstruction>) in GitHub.

<sup>11</sup> We quote error with the format of mean value  $\pm 68\%$  CL limit throughout this work if not additionally annotated.



We do not use the  $r_s$  estimates from WMAP9 and the latest Planck 18 because they are consistent with that from Planck 15 and the reconstruction results does not change as also manifested in L18. Please also note that our way of including the  $r_s$  information is different from L18 where they imposed a Gaussian prior, while we regard it as a free parameter with a flat prior.

### 3.2. Inference Method

Our constraints on the reconstruction parameters are obtained by minimizing the  $\chi^2$  function using the July 2018 version of Cosmological MonteCarlo (CosmoMC)<sup>12</sup> (Lewis & Bridle 2002; Lewis 2013) and the resulting MCMC chains are analyzed mainly using the GetDist package<sup>13</sup> (Lewis 2019). We adopt the Gelman–Rubin convergence criterion that  $R - 1 < 0.1$ . In practice, all the MCMC chains that we used to analyze have  $R - 1 \sim 0.02$ .

For a given a posterior likelihood function (PLF), the general form of  $\chi^2$  is

$$\chi^2 = -2 \ln(\text{PLF}) = \delta^T C^{-1} \delta, \quad (12)$$

where  $C$  is the covariance matrix of the data, and  $\delta$  is the difference between the data and the theoretical predictions. The second expression is valid only when the PLF are Gaussian or approximately Gaussian. If PLF is non-Gaussian, such as the GLTD data mentioned in the Section 3, then we use the general expression, i.e., the first equation.

We use the DIC to estimate the performance of the four reconstruction models. DIC combines heritage both from Akaike Information Criterion and Bayesian Information Criterion and allow for parameter degeneracy (Spiegelhalter et al. 2002; Liddle 2007). DIC is defined via

$$\text{DIC} = \overline{D(\theta)} + p_D, \quad (13)$$

where  $D(\theta) = -2 \ln \mathcal{L} + C$  and  $p_D = \overline{D(\theta)} - D(\bar{\theta})$ .  $\mathcal{L}$  is the PLF and  $C$  is a constant that only depends on data. The bars indicate averages over the posterior distribution. This definition of DIC has a clear Bayesian interpretation that deals with the average of  $\ln \mathcal{L}$  rather than the maximum values. Again,  $p_D$  has its indication that it approximately equals the effective number of parameters constrained by the data. If  $p_D$  is less than the number of free parameters of a model ( $p_M$ ), then it suggests that these model parameters are highly degenerate. For this purpose, in Table 4, we also list  $p_D/p_M$  for each models.

## 4. Results and Discussion

We impose flat priors on the model parameters, as summarized in Table 3. The constraint results are graphically presented in Figures 1–3 and the mock results are shown in Figure 5. All the numerical results are summarized in Table 4, along with three statistical quantities for model selection that are  $p_D/p_M$ , DIC, and  $\chi^2$  at best-fitting value. While  $p_D$  is a part of DIC estimate, we list it separately as it estimates the model parameter degeneracy.

<sup>12</sup> <https://github.com/cmbant/CosmoMC>

<sup>13</sup> <https://github.com/cmbant/getdist/releases/tag/1.0.0>. We also acknowledge the use of ChainConsumer package (Hinton 2016), available at <https://github.com/Samreay/ChainConsumer/tree/Final-Paper>.

**Table 3**

Summary of the Priors Imposed on Free Parameters for the Four Models

Model	Epsilon	Log	Log2	$\Omega_k \Lambda \text{CDM}$
A	[0.0, 2.0]	[0.0, 2.0]	[0.1, 0.6]	[0.1, 1.0]
B	[-2.0, 2.0]	[0.0, 2.0]	[-0.6, 0.6]	[-0.3, 0.3]
C	[-5.0, 8.0]	[-5.0, 8.0]	[0.15, 2.00]	0
D	[-2.0, 2.0]	[-10.0, 6.0]	[-1.0, 5.0]	[0.5, 1.2]
$\epsilon$	[-5.0, 5.0]	...	...	...
$r_s$	[130, 160]	[130, 160]	[130, 160]	[130, 160]

### 4.1. Constraints from Current Data

We first update the constraints on the Epsilon and Log models using the new BAO and Pantheon SN Ia. We find:

$$H_{0,\text{rec}} = 68.57 \pm 0.89, \text{ km s}^{-1} \text{ Mpc}^{-1} \text{ (68\% C.L.)}, \quad (14)$$

for the Epsilon model and

$$H_{0,\text{rec}} = 68.69 \pm 0.87, \text{ km s}^{-1} \text{ Mpc}^{-1} \text{ (68\% C.L.)}, \quad (15)$$

for the Log model. Compared to those reported in L18, the constraints on  $H_0$  are almost alike. Although two high-redshift BAO measurements are updated to the latest BOSS DR14, we do not find improvement in the accuracy mainly due to the correlation between  $H(z_{\text{eff}})$  and  $D_M$ .

Although the BAO data along with the large number of SN Ia samples can place tight constraints on the shape of  $H(z)$ , the correlations among model parameters are compelling, as shown in Figure 1, which indicates substantial redundancy of these parameters. The degeneracy in the Epsilon model is driven by the parameter  $\epsilon$ , with a double peak in the marginalized posteriors (especially obvious in Figure 1 in L18 while in our case it flattens partly because we have expand the prior range of  $B_1$  and  $D_1$  to negative ranges). Overall, the Log model shows highly correlated, however much simpler, Gaussian constraints than the Epsilon model. As indeed listed in Table 4, the effective number of the parameters in the Epsilon model is always less (by  $\sim 1$ ) than the number of free parameters in the likelihood analysis, i.e.,  $p_D/p_M < 1$ . For the Log model and other two models as well, the effective number of parameters is almost equivalent to the number of free parameters. This in turn is one of the motivations to utilize the Log model to perform the mock analysis, elaborated later.

When including the GLTD data, we find a mild shift in the posteriors distribution of parameters globally. Constraints on  $H_0$  become

$$\begin{aligned} H_{0,\text{rec}} &= 69.17 \pm 0.90, \text{ km s}^{-1} \text{ Mpc}^{-1} \text{ (68\% C.L.)}, \\ H_{0,\text{rec}} &= 69.26 \pm 0.91, \text{ km s}^{-1} \text{ Mpc}^{-1} \text{ (68\% C.L.)}, \end{aligned} \quad (16)$$

for the Epsilon model and Log model, respectively. For both models, the marginalized values of  $H_{0,\text{rec}}$  increase, drawing toward the constraint for  $w \neq -1$  extension of  $\Lambda \text{CDM}$  using the same data set, recently reported in Wong et al. (2020; see also Taubenberger et al. 2019). Preference for a higher (w.r.t CMB) value of Hubble constant from GLTD is clearly in line with other reports (e.g., Figure 2 and Table 5 in Wong et al. 2020), again in cases where the Hubble constant is determined via calibrated SNe using absolute distances from GLTD (Jee et al. 2019) and in cosmology-model-independent manners (Liao et al. 2019, 2020).

However, including GLTD does not tighten the constraints on  $H_{0,\text{rec}}$ . We expect that this is because  $H_{0,\text{rec}}$  from GLTD alone has large uncertainty and mild tension with  $H_{0,\text{rec}}$  from BAO+ $r_s$ +SN

**Table 4**Summary of the Marginalized Constraints on the Reconstruction Parameters and  $r_s$  with Upper and Lower Uncertainties at the 68% Confidence Level (CL)

Model Data Set	Epsilon		Log		Log2		$\Omega_k\Lambda$ CDM	
	SN+BAO	+GLTD	SN+BAO	+GLTD	SN+BAO	+GLTD	SN+BAO	+GLTD
A	$0.29^{+0.05}_{-0.05}$	$0.30^{+0.04}_{-0.06}$	$0.24^{+0.08}_{-0.08}$	$0.28^{+0.07}_{-0.07}$	$0.31^{+0.03}_{-0.03}$	$0.33^{+0.03}_{-0.03}$	$0.30^{+0.03}_{-0.03}$	$0.31^{+0.03}_{-0.03}$
B	$0.32^{+0.70}_{-0.87}$	$0.44^{+0.92}_{-0.80}$	$0.81^{+0.08}_{-0.09}$	$0.79^{+0.08}_{-0.08}$	$-0.02^{+0.13}_{-0.17}$	$-0.13^{+0.09}_{-0.12}$	$0.01^{+0.09}_{-0.09}$	$-0.05^{+0.07}_{-0.09}$
C	$0.08^{+1.01}_{-0.64}$	$-0.05^{+0.95}_{-0.66}$	$2.01^{+2.14}_{-2.10}$	$0.77^{+2.03}_{-1.97}$	$0.76^{+0.15}_{-0.13}$	$0.87^{+0.11}_{-0.08}$	...	...
D	$0.43^{+0.85}_{-0.83}$	$0.32^{+0.84}_{-0.99}$	$-2.00^{+2.13}_{-2.16}$	$-0.74^{+1.99}_{-2.04}$	$0.08^{+0.27}_{-0.26}$	$0.22^{+0.22}_{-0.19}$	$0.69^{+0.07*}_{-0.07}$	$0.75^{+0.07*}_{-0.05}$
$\epsilon$	$-0.17^{+2.23}_{-1.53}$	$0.13^{+1.97}_{-1.37}$	...	...	...	...	...	...
$r_s$	$147.26^{+0.30}_{-0.31}$	$147.21^{+0.30}_{-0.30}$	$147.28^{+0.31}_{-0.32}$	$147.26^{+0.28}_{-0.29}$	$147.26^{+0.32}_{-0.33}$	$147.24^{+0.29}_{-0.28}$	$147.29^{+0.32}_{-0.30}$	$147.21^{+0.33}_{-0.32}$
$H_0$	$68.57^{+0.89*}_{-0.90}$	$69.17^{+0.89*}_{-0.90}$	$68.69^{+0.86*}_{-0.84}$	$69.26^{+0.89*}_{-0.93}$	$68.53^{+0.86*}_{-0.88}$	$69.28^{+0.91*}_{-0.89}$	$68.43^{+0.91}_{-0.90}$	$69.48^{+0.97}_{-0.80}$
$p_D/p_M$	0.81	0.71	0.97	0.94	0.97	0.99	1.01	1.06
$\Delta$ DIC(DIC)	+0.66	+0.27	+0.67	+1.27	+1.49	-0.04	1047.95	1064.47
$\Delta\chi^2(\chi^2)$	-0.98	0.26	-0.88	0.36	-0.05	-1.37	1039.84	1055.95

**Note.** We impose flat prior on reconstruction parameters. We also list  $p_D/p_M$ ,  $\Delta$ DIC and  $\Delta\chi^2$  w.r.t the  $\Omega_k\Lambda$ CDM model. All derived quantities are indicated with \*. For the reference model we show the DIC and  $\chi^2$ , for which  $\Delta$ DIC =  $\Delta\chi^2 = 0$ .

Ia. Both GLTD and BAO+ $r_s$  can independently determine  $H_0$  while in the flat  $\Lambda$ CDM model their inference shows some discrepancies (Aghanim et al. 2018; Wong et al. 2020), which should be the same for the Epsilon and Log model. For example, using the Log model we plot the constraints on three parameters of interest:  $A_2$ ,  $B_2$ , and  $H_{0,\text{rec}}$  from GLTD and BAO+ $r_s$ , as well as their respective combination with SN, i.e., GLTD+SN and BAO+ $r_s$ +SN in Figure 4. As expected, the constraints from GLTD are far less stringent and numerically we get  $H_{0,\text{rec}} = 82.98 \pm 4.77$ , km s $^{-1}$  Mpc $^{-1}$ .<sup>14</sup> Please note that the above result are different from the results for the flat  $\Lambda$ CDM model shown in Section 3 because here all reconstruction parameters are free. The constraints from GLTD alone on  $A_2$  and  $B_2$  are consistent with those from BAO+ $r_s$  within the  $1\sigma$  region while on  $H_{0,\text{rec}}$ , we find a mild tension, which becomes more eye-catching when BAO+ $r_s$  is combined with SNe since the error bar shrinks significantly.

As shown in Figure 4, when contrasting the constraints from BAO+ $r_s$  (pink) against SN+GLTD (orange), it is noticeable that the correlation between  $A_2$ , which scales as the matter density and  $H_{0,\text{rec}}$ , is negative (i.e.,  $A_2 \rightarrow 0$ , for higher values of  $H_{0,\text{rec}}$ ) for the former and positive for the latter data set. This results in a lower value of  $H_{0,\text{rec}}$  in their joint analysis and demonstrates why a low-redshift modification, as in the case of a parametric Log model cannot resolve the  $H_0$ -tension. Similar behavior was also earlier noted in Bernal et al. (2016; see their Table 4 therein), using spline based reconstructions, where the SN data along with a Planck  $r_s$  disfavored higher values of  $H_0$ , also validating the adequate utility of parametric reconstructions employed here.

Next, we consider the Log2 and  $\Omega_k\Lambda$ CDM models with a curvature term in both of their parametric expressions. Figure 2 shows the constraint contours for Log2 model, which are quite similar yet with a reduced degeneracy in comparison to the Log model due to the replacement of the linear term with the quadrature/curvature term. The shape of  $H(z)$  for the Log and Log2 model show a major difference at high redshifts, where the Log model falls faster with its error bars tending to diverge. While it is not visible when plotting with the  $z$ -axis in logarithmic, we find that the Log model is, in fact, better driven by the data, which is not the case for the Log2 model, whose  $H(z)$

evolves more gradually at both extremes of redshift range. This data driven behavior further affirms the aforementioned motivation based on an effective number of constrained parameters to utilize the Log model to perform the mock analyses. Also for the Log model we find almost no variation in  $p_D/p_M \sim 1$  with the inclusion of the GLTD data set being very close to the number of free parameters in the likelihood analysis. However, we notice that the Log model provides slightly conservative constraints on  $H_{0,\text{rec}}$ , owing to its different behavior with the GLTD data set.

The  $\Omega_k\Lambda$ CDM model is the most optimal fit with the smallest DIC if we only consider BAO+ $r_s$ +SN Ia, essentially due to the smallest number of free parameters while having only slightly larger  $\chi^2$  values than the other models. If including the GLTD, then the Log2 model is optimal by a narrow margin, whose best-fit  $\chi^2$  value becomes small enough to offset the penalty in DIC due to one more extra parameter than the  $\Omega_k\Lambda$ CDM model. We further find that for the first three models,  $p_D$  always becomes smaller when GLTD is included, which is mostly due to the fact that GLTD is in mild tension with BAO+ $r_s$ +SN Ia, as shown in Figure 4. Including GLTD would actually increase the freedom, i.e., the degeneracy of free parameters allowed solely by BAO and SN Ia.

#### 4.2. Discussion of the Current Constraints

The constraining ability of combined data sets on the four models is even, having negligible difference in  $H_{0,\text{rec}}$  estimates. For the Log model, the  $H_{0,\text{rec}}$  in comparison to the Planck  $\Lambda$ CDM<sup>15</sup> and local measurement<sup>16</sup> are at  $\sim 1.3\sigma$ <sup>17</sup> using SN+BAO (1.8 $\sigma$  using SN+BAO+GLTD) and  $\sim 2.6\sigma$  (2.2 $\sigma$ ), respectively. Although the value of  $H_{0,\text{rec}}$  is slightly raised by GLTD, the increment is too small to be consistent with the

<sup>15</sup> For the same Planck likelihood combination utilized for estimating  $r_s$  here, the corresponding 68% CL limit is  $H_0 = 67.27 \pm 0.66$ , km s $^{-1}$  Mpc $^{-1}$ , for the  $\Lambda$ CDM model.

<sup>16</sup> We adopt the value of  $H_0 = 73.45 \pm 1.66$ , km s $^{-1}$  Mpc $^{-1}$ , from Riess et al. (2018; hereafter R18).

<sup>17</sup> As is the usual practice in an inverse distance ladder comparison, we assume no correlation between our  $H_{0,\text{rec}}$  and Planck  $H_0$ , however, the Planck  $r_s$  is strongly (+0.79) correlated to the latter and our  $r_s$  posterior is mildly (-0.14) anti-correlated with the former while being equivalent to the estimate. Implying  $\sim -0.12$  anti-correlation between the two  $H_0$  quantities and is expected to increase the deviation and might have a role to play with more precise future data, for instance, increasing to -0.27, in the forecast analysis presented in Section 4.3.

<sup>14</sup> For other three models, i.e., the Epsilon, Log2, and  $\Omega_k\Lambda$ CDM,  $H_{0,\text{rec}}$  with its corresponding 68% CL are  $80.61 \pm 5.53$ , km s $^{-1}$  Mpc $^{-1}$ ,  $76.58 \pm 3.46$ , km s $^{-1}$  Mpc $^{-1}$ , and  $74.26 \pm 2.57$ , km s $^{-1}$  Mpc $^{-1}$ , respectively.

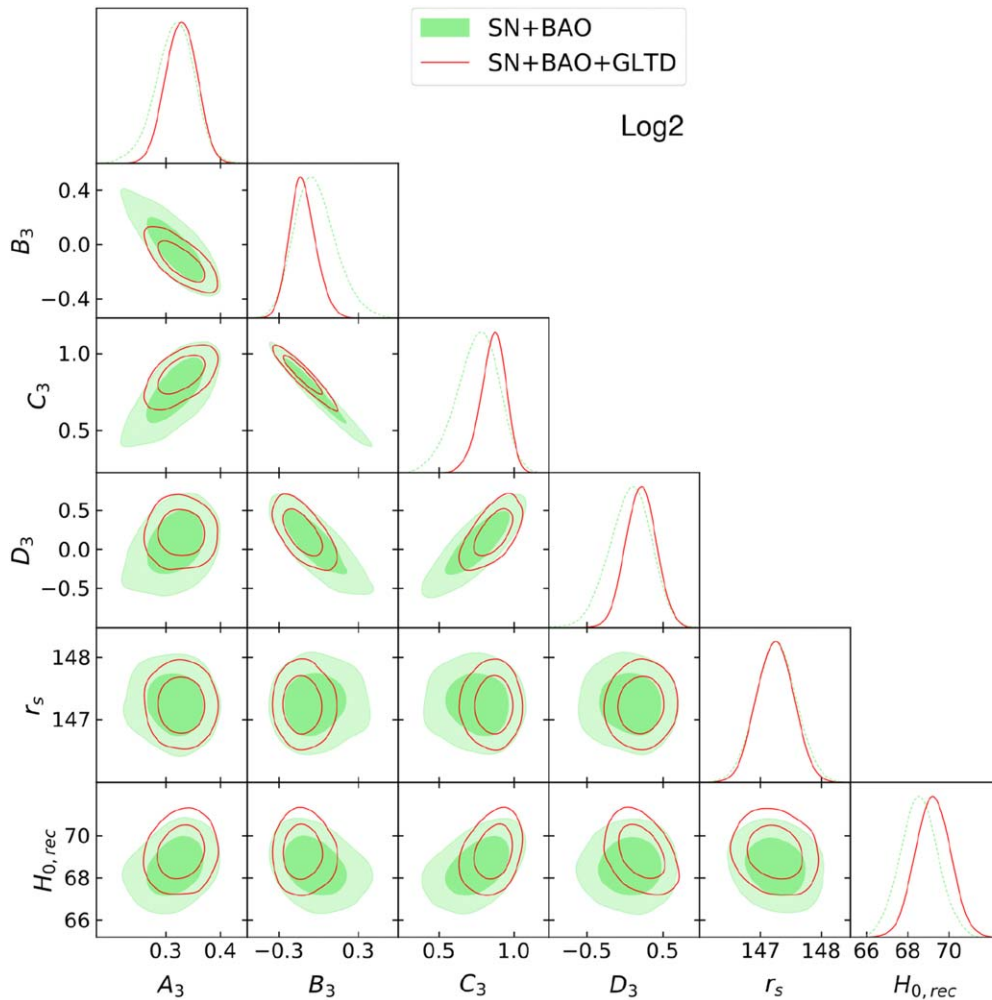


**Figure 2.** Parameter constraints for the Log2 model at 68% and 95% CL limits. Here the parameter  $B_3$  corresponds to curvature. We also show the reconstructed  $H_{0,rec}$ .

local measurement of  $H_0$ . While this situation would change if the GLTD becomes more accurate and precise, at the current stage, our reconstructed Hubble constant still favors the Planck estimate, which is in agreement with other earlier analyses (Aubourg et al. 2015; Bernal et al. 2016; Feeney et al. 2018). We also notice that the  $H_0$  estimates in our analyses, driven by the combination of GLTD data and Planck  $r_s$  are extremely consistent with those reported in Haridasu et al. (2018a), Gómez-Valent & Amendola (2018), Mukherjee et al. (2019), and Dutta et al. (2019),<sup>18</sup> which were driven by Cosmic Chronometers (CC) data sets. These earlier results are also model-independent, being very different from the approach implemented here. The low-redshift model-independent (see, e.g., Haridasu et al. 2018a) constraint on the compound parameter  $r_s \times H_0 / [100, \text{km s}^{-1} \text{Mpc}^{-1}] (r_s h)$  is consistent with the Planck estimate within  $1\sigma$ .

We notice that if we put any information from CMB aside and just use the three low-redshift data (SN, BAO, and GLTD), thanks to the sensitivity of GLTD data to  $H_0$ , which is used to break the degeneracy between  $r_s$  and  $H_0$  existing in the BAO data, we can obtain an estimate of  $r_s$  that is completely independent of physics

of the early universe. Then for the Log model, the constraints on  $H_0$  and  $r_s h$  are  $74.74 \pm 2.01, \text{km s}^{-1} \text{Mpc}^{-1}$  and  $101.29 \pm 1.34 \text{Mpc}$ , respectively, while the former is consistent with the local measurement and the latter is only off the Planck estimate ( $r_s h = 99.069 \pm 1.598 \text{Mpc}$ , obtained from the same combination of Planck likelihood as  $r_s$ ) at  $\sim 1\sigma$  level. The resulting  $r_s$  is  $135.60 \pm 3.64 \text{Mpc}$ . This result is very similar to Aylor et al. (2019) while in our case we also combined with the GLTD and as also suggested in Knox & Millea (2020) such results imply a lower sound horizon from CMB data.

Please note that fixing  $r_s$  from CMB will be equivalent to a one-parameter extension such as,  $\Omega_k \neq 0$  or  $w \neq -1$ , i.e., it will result in the same early-time behavior. We utilize the same  $r_s$  value for all models implemented here with different late-time behavior, ideally expecting a different  $r_s h$  w.r.t.  $\Lambda\text{CDM}$ . On the other hand, the  $r_s h$  would imply a correlated early ( $r_s$ ) and late-time ( $H_0$ ) behavior while fixing the angular scales measured by CMB. An agreement on  $r_s h$  constraint from these three low-redshift data and high-redshift CMB, alongside the conformity of higher (than CMB)  $H_0$  values from local distance ladder (R18, Riess et al. 2019) and GLTD (Wong et al. 2020) data sets<sup>19</sup> at a face value indicates a need

<sup>18</sup> See for example, other works driven by CC based  $H_0$  estimations (Luković et al. 2016, 2018; Yu et al. 2018; Park & Ratra 2019), which at times do not account for the systematics within CC data.

<sup>19</sup> Please see Verde et al. (2019) and Riess (2019) for a summary of other low-redshifts probes which imply similar  $H_0$  estimates.

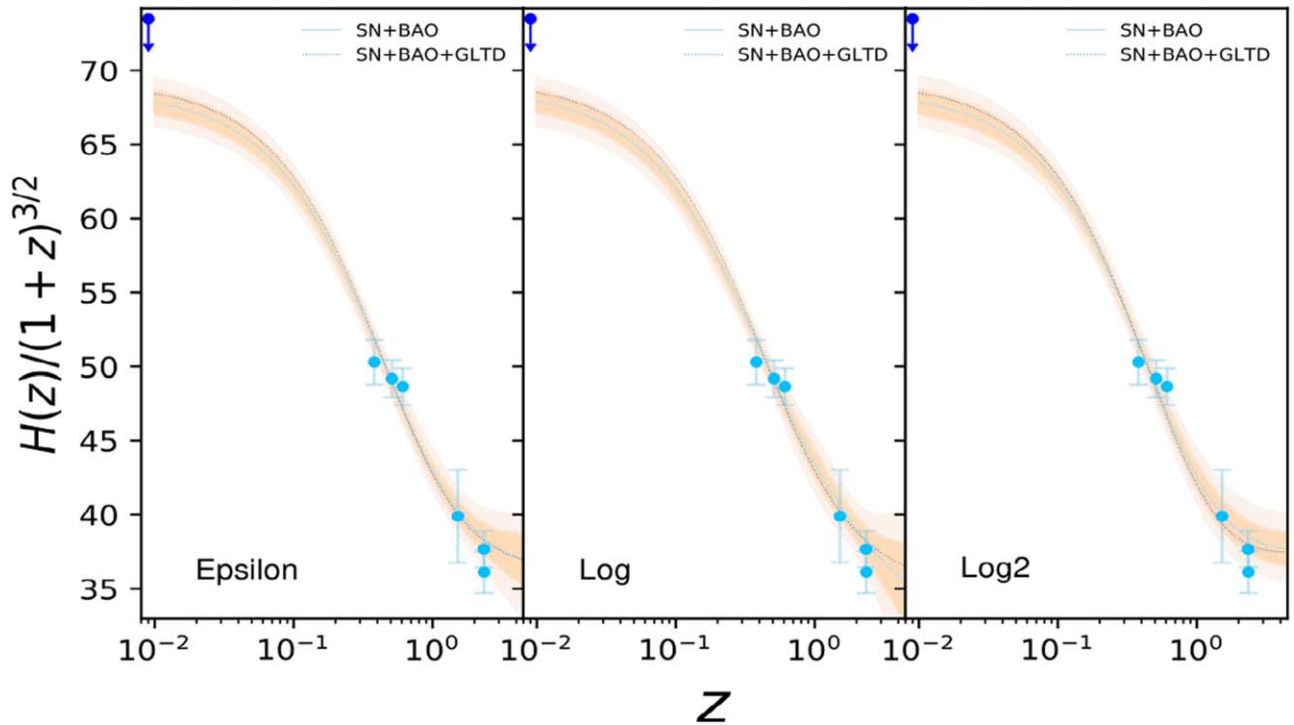


**Figure 3.** Evolution of reconstructed  $H(z)$  with the  $z$ -axis in log scale with truncation at  $z = 4.5$ . The shaded region is the  $1\sigma$  and  $2\sigma$  error range of the joint constraint from Pantheon SN Ia+BAO+GLTD. The light blue points are the BAO estimates of  $H(z)$  with its  $1\sigma$  error. The blue point is the local  $H_0$  measurements and its lower  $1\sigma$  limit from the distance ladder (Riess et al. 2018). When including GLTD, a rise of  $H(z)$  in the low-redshift range appears for all models, which results in a slightly higher  $H_{0,\text{rec}} \sim 0.6$ , which is in accordance with the fact that BAO data along with the Planck  $r_s$  supersedes the precision with which the GLTD data constrain the present expansion rate.

for modification of early-time physics (see Knox & Millea (2020) for a more detailed discussion) as a desirable solution for the  $H_0$ -tension.

#### 4.3. Constraints from Future Data

While the analyses so far, with the up-to-date BAO and GLTD data, reaffirm the inferences of L18, we are now more interested in forecasting the constraining ability of future BAO and GLTD data sets on  $H_0$  through the model-independent formalism. While several surveys in contemplation such as Euclid (Amendola et al. 2018) and the Square Kilometre Array (Bacon et al. 2018) can provide precise measurements on BAO (Obuljen et al. 2018; Bengaly et al. 2019), here we focus on BAO from DESI. As for the GLTD simulation, we consider the LSST.

DESI is a Stage IV ground-based experiment that started in 2019.<sup>20</sup> It aims at studying BAO and the growth of structure through measuring spectra from four target tracers, including luminous red galaxies up to  $z \sim 1.0$ , bright [O II] emission line galaxies up to  $z \sim 1.7$ , quasars and Ly $\alpha$  forest absorption feature in their spectrum up to  $z = 3.5$ . Following Aghamousa et al. (2016), we use 18 DESI BAO measurements from their baseline 14K survey, which are quoted as  $D_A(z)/r_s$  and  $H(z)r_s$ , 15 of which come from the basic galaxy and quasar BAO distance measurement projections (Table 2.3 therein) and the remaining 5 from the bright galaxy survey (Table 2.5).<sup>21</sup> We

<sup>20</sup> <https://www.desi.lbl.gov/>

<sup>21</sup> We found that, if only the BAO data is simulated, the accuracy of  $H_{\text{rec},0}$  is only improved by  $\sim 3\%$  if after including the Ly $\alpha$  forest data assuming that these two measurements are independent. Also, we do not find information about the correlation coefficient in the literature. So we do not use DESI Ly $\alpha$  forest data.

assume a correlation coefficient of 0.4 between  $D_A(z)/r_s$  and  $H(z)r_s$  as proposed in Aghamousa et al. (2016).

LSST is an ambitious wide-deep-fast sky survey that plans for regular survey operations by 2022 (Ivezic et al. 2019). Oguri & Marshall (2010) made predictions of the numbers of time-variable sources that should be found by LSST and reported a very positive result that around 3000 lensed quasars will have well-measured time delays. Based on the catalog of mock lenses in Oguri & Marshall (2010), Jee et al. (2016) further forecast that  $\sim 55$  high-quality quadruple lens systems would have sufficiently good measurements of both  $D_{\Delta t}$  and  $D_d$  and in turn, could put strong cosmographic constraints. However, this number may vary due to various limitations such as the telescope observation strategy (Liao 2019). Furthermore, there should be correlations between the measured  $D_{\Delta t}$  and  $D_d$  estimates or otherwise one of the distances will have much uncertainty. Due to the lack of correlation information, in their paper, here we assume that only  $D_{\Delta t}$  is available. According to the current six GLTD observations, the uncertainty on  $D_{\Delta t}$  varies within  $\sim 4.0\% - 8.0\%$ . A 5% uncertainty level is practically achievable as long as we select the lens systems following the same criteria as Jee et al. (2016). The number of forecasted lens systems is conservatively reduced to 40.

The top panel of Figure 5 shows the 1D marginalized posterior of inferred  $H_0$  when combining the current data with the future BAO and GLTD data for the Log model, with the Planck  $r_s$  estimate, where the relative heights are also indicative of the constraining ability of the data. For convenient comparison, we plot the current constraint in dotted gray. We do not analyze the other three models in detail, as they are not expected to exhibit much difference, and we verify that the



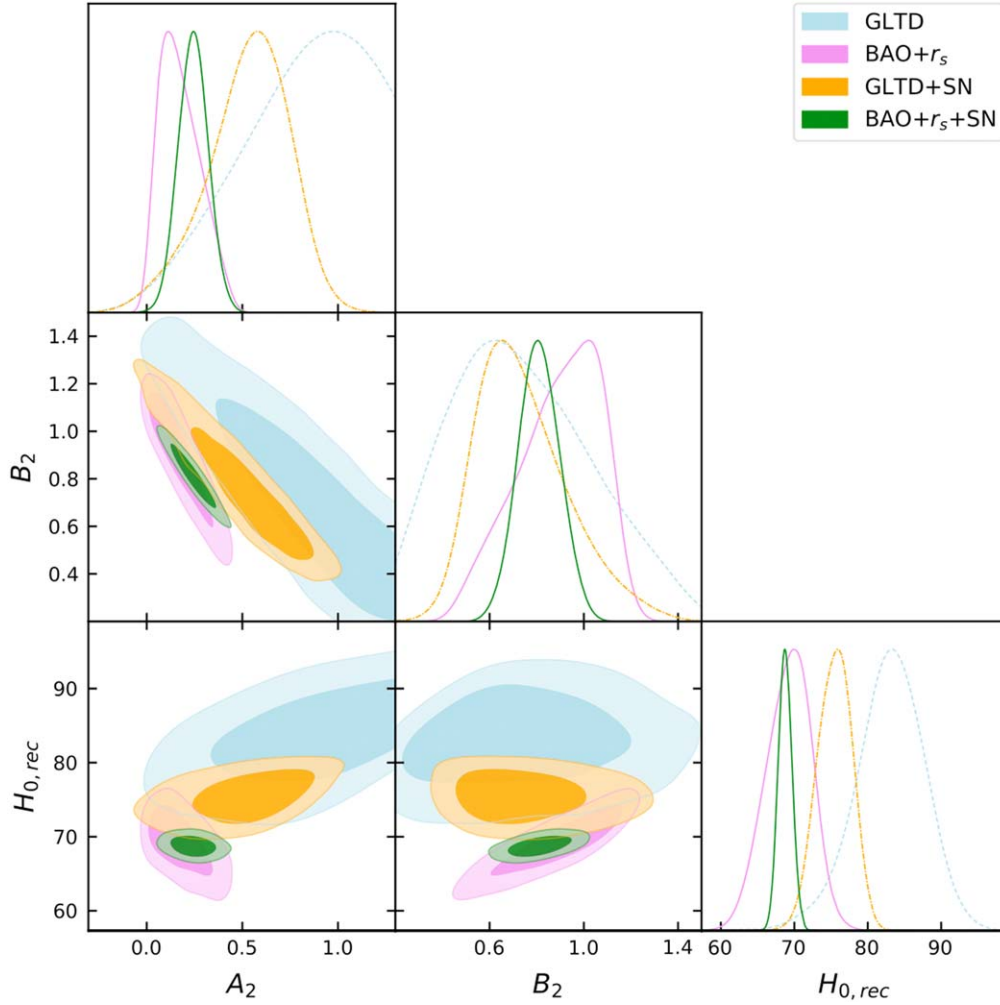


**Figure 4.** Comparison of constraint results of different data sets for the Log model. All parameters of the Log model are free. Here we only report parameters of most interest,  $A_2$ ,  $B_2$ , and  $H_{0,rec}$  (see the discussion in the text).

improvement in percentages will remain the same. However, testing the Epsilon model we find that it is less reliable to reproduce the model utilized to create the mock data set, due to stronger intrinsic degeneracy among the parameters.

With the fiducial model being the best-fitting value constrained by the current BAO data with the Planck  $r_s$  estimate, we forecast the performance of upcoming DESI data. We find the uncertainty on  $H_{0,rec}$  shrinks by a factor of  $\sim 2.3$  (from 3.1 to 1.4), i.e., reduces by  $\sim 56\%$ , which is quite encouraging. The improvement in the uncertainty of  $H_{0,rec}$  when the current data (SN+BAO+GLTD) are combined with LSST GLTD, DESI BAO, and LSST GLTD+DESI BAO are  $\sim 13.0\%$ ,  $24.4\%$ , and  $26.7\%$ , respectively, reaching  $\sigma_{H_{0,rec}} \approx 0.67$  uncertainty level finally. Our estimate of the improved  $\sigma_{H_{0,rec}} \approx 0.80$  with the inclusion of forecasted GLTD data alone is in agreement with the analysis in Jee et al. (2016).<sup>22</sup>

Tentatively, the improved precision obtained with the future data (DESI+LSST) around the current best-fit model would imply similar disagreements at the level of  $\sim 2.1\sigma$  higher and  $\sim 2.3\sigma$  lower than the Planck  $\Lambda$ CDM and R18  $H_0$  derived values, respectively. This could imply a possibility for low-redshift ( $0.1 \leq z \leq 2.5$ )  $H_0$  estimate that lies between the local

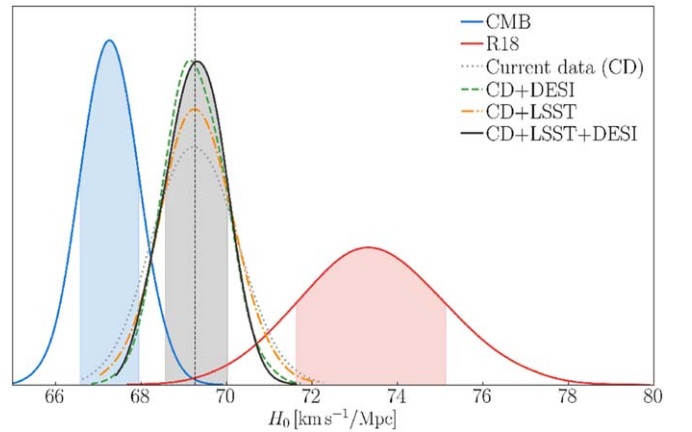


**Figure 5.** Forecasts of marginalized  $H_0$  using the future data, i.e., BAO from DESI and GLTD data from LSST. We choose the fiducial model following the best-fitting of the joint constraint from Pantheon SN Ia, BAO, and GLTD (i.e., current data). The vertical dashed line represents the mean value from the posterior.

( $z \leq 0.15$ ) and high-redshift CMB estimate. As also shown in the top panel of Figure 5, the DESI BAO data contribute most to reducing the uncertainty. The LSST GLTD data are important as well, but they are overwhelmed by the BAO data

<sup>22</sup> A more recent analysis in Shiralilou et al. (2020) forecasts GLTD performance in an ideal scenario, which we do not compare with here.

when combined. Please note that we have not considered the additional distance information of  $D_d$  from the future GLTD measurements. According to Jee et al. (2016), including the  $D_d$  distance would improve the constraint significantly. An earlier forecast shows about 400 systems of robust measured time delay should be discovered by LSST (Liao et al. 2015). We expect the future GLTD data will have a better performance than our relatively conservative anticipation. In addition, please note that with the the fiducial cosmology to create the mock data sets being the best-fit of Log model to the current data, we do not study the contest between the GLTD and BAO data sets, but only forecast the precision of the joint constraint from the future low-redshift data.

## 5. Summary

In the current work, we reconstruct the late-time expansion history of the universe in a cosmological-model-independent way, focusing on the Hubble constant  $H_0$ , using the latest SN Ia, BAO, and GLTD data, implementing four different parametric forms. A summary of our results is as follows:

1. Assuming the Gaussian  $r_s$  from the high-redshift Planck estimate for  $\Lambda$ CDM, our deduced value of Hubble constant for the four models are more consistent with the Planck  $\Lambda$ CDM, e.g., for the Log model, at  $\sim 1.3\sigma$  using SN+BAO ( $1.8\sigma$  using SN+BAO+GLTD) estimate than with the higher-valued local measurement at  $\sim 2.6\sigma$  ( $2.2\sigma$  using SN+BAO+GLTD). We assess the performance of the parametric models and find no preference among models having comparable values of DIC.
2. With the updated data and also a curvature freedom (Log2 model), we reaffirm the conclusions of L18, that the Hubble tension possibly originates from the early universe. However, as the reconstructed  $H(z)$ , and hence  $H_{0,\text{rec}}$ , is driven by the data (within the available freedom of the parametric models), conclusions remain to be verified with more stringent future data.
3. Inclusion of GLTD data only mildly increases the best-fitting value of  $H_{0,\text{rec}}$ , hardly improving uncertainty, due to the considerably lower constraining power of GLTD data. We assess mild disagreements among low-redshift data combinations. It is expected to yield possibly increased disagreements with the updated GLTD data set in Wong et al. (2020).
4. More importantly, we anticipate the performance of future BAO and GLTD data from two upcoming experiments, DESI and LSST. When combined with the current data, we infer an improvement in the uncertainty of  $H_0$  by  $\sim 13.0\%$  and  $\sim 24.4\%$ , with GLTD and BAO data, respectively. Combining these two future data will provide an improvement in precision by  $\sim 26.7\%$ , and might incite a need for agreement between local ( $z \leq 0.15$ ), low-redshift ( $0.10 \leq z \leq 2.5$ ), and high-redshift (CMB)  $H_0$  estimates, indicating moderate-level ( $\ll 9\%$  of current difference) modifications to both the CMB and local  $H_0$  estimates.

Implementing a multitude of contrasting analyses in a model-independent inverse distance ladder framework, we expect to find a strong degree of complementarity between BAO and GLTD data sets in the near future, which will provide tighter constraints on cosmological models, and also highlight

much-needed prospects to resolve the  $H_0$ -tension and further important evidence to test physically motivated extensions to the  $\Lambda$ CDM model.

This work was supported by the National Natural Science Foundation of China under grants Nos. U1931202, 11633001, and 11690023. M.V. is supported by INFN INDARK PD51 grant and agreement ASI-INAF n.2017-14-H.0. B.S.H. acknowledges financial support by ASI grant No. 2016-24-H.0.

## ORCID iDs

Meng-Zhen Lyu  <https://orcid.org/0000-0002-0229-3439>

## References

- Abbott, T. M. C., Allam, S., Andersen, P., et al. 2019, *ApJL*, 872, L30
- Ade, P. A. R., Agnaim, N., Armitage-Caplan, C., et al. 2014, *A&A*, 571, A16
- Ade, P. A. R., Agnaim, N., Arnaud, M., et al. 2016, *A&A*, 594, A13
- Aghamousa, A., Aguilar, J., Ahlen, S., et al. 2016, arXiv:1611.00036
- Aghanim, N., Akrami, Y., Ashdown, M., et al. 2018, arXiv:1807.06209
- Alam, S., Ata, M., Bailey, S., et al. 2017, *MNRAS*, 470, 2617
- Amendola, L., Appleby, S., Avgoustidis, A., et al. 2018, *LRR*, 21, 2
- Archidiacono, M., Hooper, D. C., Murgia, R., et al. 2019, *JCAP*, 1910, 055
- Aubourg, É., Bailey, S., Bautista, J. E., et al. 2015, *PhRvD*, 92, 123516
- Aylor, K., Joy, M., Knox, L., et al. 2019, *ApJ*, 874, 4
- Bacon, D. J., Battye, R. A., Bull, P., et al. 2018, *PASA*, 37, e007
- Ballardini, M., Finelli, F., Umiltà, C., & Paoletti, D. 2016, *JCAP*, 2016, 067
- Banihashemi, A., Khosravi, N., & Shirazi, A. H. 2019, *PhRvD*, 99, 083509
- Bautista, J. E., Vargas-Magaña, M., Dawson, K. S., et al. 2018, *ApJ*, 863, 110
- Bengaly, C. A. P., Clarkson, C., & Maartens, R. 2019, arXiv:1908.04619
- Bernal, J. L., Verde, L., & Riess, A. G. 2016, *JCAP*, 2016, 019
- Betoung, M., Kessler, R., Guy, J., et al. 2014, *A&A*, 568, A22
- Beutler, F., Blake, C., Colless, M., et al. 2011, *MNRAS*, 416, 3017
- Birrer, S., Treu, T., Rusu, C., et al. 2019, *MNRAS*, 484, 4726
- Blomqvist, M., du Mas des Bourboux, H., Busca, N. G., et al. 2019, *A&A*, 629, A86
- Camera, S., Martinelli, M., & Bertacca, D. 2019, *PDU*, 23, 100247
- Chen, G. C.-F., Fassnacht, C. D., Suyu, S. H., et al. 2019, *MNRAS*, 490, 1743
- Choi, G., Suzuki, M., & Yanagida, T. T. 2019, arXiv:1910.00459
- Clarkson, C., Cortès, M., & Bassett, B. 2007, *JCAP*, 2007, 011
- de Sainte Agathe, V., Balland, C., du Mas des Bourboux, H., et al. 2019, *A&A*, 629, A85
- di Valentino, E., Boehm, C., Hivon, E., & Bouchet, F. M. C. R. 2018a, *PhRvD*, 97, 043513
- di Valentino, E., Linder, E. V., & Melchiorri, A. 2018b, *PhRvD*, 97, 043528
- di Valentino, E., Melchiorri, A., Linder, E. V., & Silk, J. 2017a, *PhRvD*, 96, 023523
- di Valentino, E., Melchiorri, A., & Mena, O. 2017b, *PhRvD*, 96, 043503
- Dutta, K., Roy, A., Ruchika, S. A. A., & Sheikh-Jabbari, M. M. 2019, *PhRvD*, 100, 103501
- Feeney, S. M., Mortlock, D. J., & Dalmaso, N. 2018, *MNRAS*, 476, 3861
- Gómez-Valent, A., & Amendola, L. 2018, *JCAP*, 2018, 051
- Haridasu, B. S., Luković, V. V., Moresco, M., & Vittorio, N. 2018a, *JCAP*, 1810, 015
- Haridasu, B. S., Luković, V. V., & Vittorio, N. 2018b, *JCAP*, 5, 033
- Hinton, S. R. 2016, *JOSS*, 1, 00045
- Hoscheit, B. L., & Barger, A. J. 2017, AAS Meeting, 230, 314.05
- Huang, Q.-G., & Wang, K. 2016, *EPJC*, 76, 506
- IcazaLizaola, M., Vargas-Magaña, M., Fromenteau, S., et al. 2020, *MNRAS*, 492, 4189
- Ivezic, Z., Kahn, S. M., Tyson, J. A., et al. 2019, *ApJ*, 873, 111
- Jee, I., Komatsu, E., Suyu, S., & Huterer, D. 2016, *JCAP*, 2016, 031
- Jee, I., Komatsu, E., & Suyu, S. H. 2015, *JCAP*, 1511, 033
- Jee, I., Suyu, S., Komatsu, E., et al. 2019, *Sci*, 365, 1134
- Karwal, T., & Kamionkowski, M. 2016, *PhRvD*, 94, 103523
- Keenan, R. C., Barger, A. J., & Cowie, L. L. 2013, *ApJ*, 775, 62
- Kenworthy, W. D., Scolnic, D., & Riess, A. 2019, *ApJ*, 875, 145
- Khosravi, N., Baghram, S., Afshordi, N., & Altamirano, N. 2019, *PhRvD*, 99, 103526
- Knox, L., & Millea, M. 2020, *PhRvD*, 101, 043533
- Ko, P., & Tang, Y. 2016, *PhLB*, 762, 462
- Kumar, S., & Nunes, R. C. 2016, *PhRvD*, 94, 123511
- Lemos, P., Lee, E., Efstathiou, G., & Gratton, S. 2019, *MNRAS*, 483, 4803

- Levi, M., Bebek, C., Beers, T., et al. 2013, arXiv:1308.0847
- Lewis, A. 2013, [PhRvD](#), **87**, 103529
- Lewis, A. 2019, arXiv:1910.13970
- Lewis, A., & Bridle, S. 2002, [PhRvD](#), **66**, 103511
- Liao, K. 2019, [ApJ](#), **883**, 3
- Liao, K., Shafieloo, A., Keeley, R. E., & Linder, E. V. 2019, [ApJL](#), **886**, L23
- Liao, K., Shafieloo, A., Keeley, R. E., & Linder, E. V. 2020, arXiv:2002.10605
- Liao, K., Treu, T., Marshall, P., et al. 2015, [ApJ](#), **800**, 11
- Liddle, A. R. 2007, [MNRAS](#), **377**, L74
- Luković, V. V., D'Agostino, R., & Vittorio, N. 2016, [A&A](#), **595**, A109
- Luković, V. V., Haridasu, B. S., & Vittorio, N. 2018, [FoPh](#), **48**, 1446
- Luković, V. V., Haridasu, B. S., & Vittorio, N. 2020, [MNRAS](#), **491**, 2075
- Marra, V., Amendola, L., Sawicki, I., & Valkenburg, W. 2013, [PhRvL](#), **110**, 241305
- Mortsell, E., & Dhawan, S. 2018, [JCAP](#), **1809**, 025
- Mukherjee, A., Paul, N., & Jassal, H. K. 2019, [JCAP](#), **2019**, 005
- Narayan, R. 1991, [ApJL](#), **378**, L5
- Obuljen, A., Castorina, E., Villaescusa-Navarro, F., & Viel, M. 2018, [JCAP](#), **2018**, 004
- Oguri, M., & Marshall, P. J. 2010, [MNRAS](#), **405**, 2579
- Pan, S., Yang, W., di Valentino, E., Saridakis, E. N., & Chakraborty, S. 2019, [PhRvD](#), **100**, 103520
- Paraficz, D., & Hjorth, J. 2009, [A&A](#), **507**, 49
- Park, C.-G., & Ratra, B. 2019, [Ap&SS](#), **364**, 82
- Poulin, V., Boddy, K. K., Bird, S., & Kamionkowski, M. 2018, [PhRvD](#), **97**, 123504
- Poulin, V., Smith, T. L., Karwal, T., & Kamionkowski, M. 2019, [PhRvL](#), **122**, 221301
- Raveri, M., & Hu, W. 2019, [PhRvD](#), **99**, 043506
- Raveri, M., Hu, W., Hoffman, T., & Wang, L.-T. 2017, [PhRvD](#), **96**, 103501
- Riess, A. G. 2019, [NatRP](#), **2**, 10
- Riess, A. G., Casertano, S., Yuan, W., et al. 2018, [ApJ](#), **855**, 136
- Riess, A. G., Casertano, S., Yuan, W., Macri, L. M., & Scolnic, D. 2019, [ApJ](#), **876**, 85
- Riess, A. G., Macri, L. M., Hoffmann, S. L., et al. 2016, [ApJ](#), **826**, 56
- Rossi, M., Ballardini, M., Braglia, M., et al. 2019, [PhRvD](#), **100**, 103524
- Rusu, C. E., Wong, K. C., Bonvin, V., et al. 2020, [MNRAS](#), **tmp**, 1660
- Scolnic, D. M., Jones, D. O., Rest, A., et al. 2018, [ApJ](#), **859**, 101
- Shanks, T., Hogarth, L. M., & Metcalfe, N. 2019, [MNRAS](#), **484**, L64
- Shirailou, B., Martinelli, M., Papadomanolakis, G., et al. 2020, [JCAP](#), **4**, 057
- Spiegelhalter, D. J., Best, N. G., Carlin, B. P., & van der Linde, A. 2002, *Journal of the Royal Statistical Society: Series b (Statistical Methodology)*, **64**, 583
- Suyu, S. H., Marshall, P. J., Auger, M. W., et al. 2010, [ApJ](#), **711**, 201
- Suyu, S. H., Treu, T., Hilbert, S., et al. 2014, [ApJL](#), **788**, L35
- Taubenberger, S., Suyu, S. H., Komatsu, E., et al. 2019, [A&A](#), **628**, L7
- Treu, T., & Marshall, P. J. 2016, [A&ARv](#), **24**, 11
- Umiltà, C., Ballardini, M., Finelli, F., & Paoletti, D. 2015, [JCAP](#), **2015**, 017
- Vagnozzi, S. 2020, [PhRvD](#), **102**, 023518
- Verde, L., Bellini, E., Pigozzo, C., Heavens, A. F., & Jimenez, R. 2017a, [JCAP](#), **2017**, 023
- Verde, L., Bernal, J. L., Heavens, A. F., & Jimenez, R. 2017b, [MNRAS](#), **467**, 731
- Verde, L., Treu, T., & Riess, A. G. 2019, [NatAs](#), **3**, 891
- Whitbourn, J. R., & Shanks, T. 2014, [MNRAS](#), **437**, 2146
- Wong, K. C., Suyu, S. H., Auger, M. W., et al. 2016, [MNRAS](#), **465**, 4895
- Wong, K. C., Suyu, S. H., Chen, G. C. F., et al. 2020, [MNRAS](#), **tmp**, 1661
- Xia, J.-Q., Li, H., & Zhang, X. 2013, [PhRvD](#), **88**, 063501
- Xia, J.-Q., & Viel, M. 2009, [JCAP](#), **2009**, 002
- Yang, W., Pan, S., di Valentino, E., et al. 2018, [JCAP](#), **1809**, 019
- Ye, G., & Piao, Y.-S. 2020, [PhRvD](#), **101**, 083507
- Yu, H., Ratra, B., & Wang, F.-Y. 2018, [ApJ](#), **856**, 3
- Yuan, W., Riess, A. G., Macri, L. M., Casertano, S., & Scolnic, D. 2019, arXiv:1908.00993
- Zarrouk, P., Burtin, E., Gil-Marín, H., et al. 2018, [MNRAS](#), **477**, 1639
- Zhao, M.-M., He, D.-Z., Zhang, J.-F., & Zhang, X. 2017, [PhRvD](#), **96**, 043520